2023-05

Serviceability behaviour of FRP-reinforced slatted slabs made of high-content recycled aggregate concrete

Imjai, T

10.1016/j.istruc.2023.03.075
Structures
Elsevier BV

Serviceability behaviour of FRP-reinforced slatted slabs made of high-content recycled aggregate concrete

Thanongsak IMJAI [1,*], Reyes GARCIA [2], Boksun KIM [3], Chayanon HANSAPINYO [4], and Piti SUKONTASUKKUL[5]

[1] *School of Engineering and Technology, Walailak University, Nakhonsithammarat 80161, Thailand2*
[2] *Civil Engineering Stream, School of Engineering, The University of Warwick, Coventry, UK CV4 7AL*
[3] *School of Engineering, Computing & Mathematics, University of Plymouth, Plymouth, PL4 8AA, UK*
[4] *Excellence Center in Infrastructure Technology and Transportation Engineering (ExCITE), Department of Civil Engineering, Chiang Mai University, Chiang Mai 50200, Thailand*
[5] *Construction and Building Materials Research Center, Department of Civil Engineering, Faculty of Engineering, King Mongkut University of Technology North Bangkok, Thailand*
([*]Corresponding author's e-mail: thanongsak.im@wu.ac.th)

Abstract

This article investigates experimentally and numerically the serviceability behaviour of FRP-reinforced slatted slabs cast with recycled aggregate concrete (RAC). Fifteen slabs were tested in three Series: a) Series normal concrete (NC) cast with natural aggregate concrete, b) Series 50RAC cast with a concrete made with 50% recycled concrete aggregate, and c) Series 100RAC cast with a concrete made with 100% recycled concrete aggregate. All slabs were subjected to four-point bending until failure. The test results are then compared to crack widths and deflection predictions given by current guidelines and Nonlinear Finite Element Analysis (FEA). The results show that the predictions given by ACI 440.1R underestimate the experimental deflections by up to 30% at maximum load levels. The sum of the flexural deflections given by Eurocode 2 and of the shear crack-induced deflections (calculated using equations proposed recently by the authors) match better the experimental deflections at both the onset of diagonal shear cracking load, and at the maximum load. The Concrete Damage Plasticity (CDP) model adopted in the FEA was suitable to predict accurately the deformations of FRP RAC slabs. This study contributes towards the development of new more sustainable structural solutions for FRP RAC elements, as well as towards more accurate models to calculate their deflections.

Keywords: Recycled concrete aggregate; FRP; Slatted slabs; Serviceability; Deflections.

Accepted on March 13, 2023 by Structures.
https://doi.org/10.1016/j.istruc.2023.03.075

1. Introduction

Over the last decades, the amount of demolition waste from construction has increased significantly, which in turn has created environmental issues in many countries. Most of the demolition waste consists of materials that can be reused or recycled. In particular, recycled concrete aggregate (RCA) can be used to produce new recycled aggregate concrete (RAC) elements [1–4]. The use of RCA as a replacement of natural aggregate (NA) impacts positively the environment, reduces the carbon footprint and improves the use of natural resources [5–8]. Whilst early uses of RCA ware mainly in road construction [9–12], the sustainability agenda in the construction industry has positioned RCA as a feasible option to replace NA in new structural concretes.

Numerous studies have examined the behaviour of structural elements made with RAC containing different amounts of RCA [13–21]. Overall, the results indicate that the use of RCA degrades the mechanical properties of the new RAC. This can be attributed to the high porosity of RCA, which also contains residues of mortar and surface cracks [14, 15, 19, 20]. For instance, the compressive strength of RAC can decrease by up to 30% when the RCA replaces 100% of the NA [14, 21–23]. As a result, maximum RCA replacement levels of 20-25% have been suggested so that new RAC can retain most of its strength and workability [13, 15–16, 21, 22, 24]. This is also reflected in current guidelines [25-27] which limit the maximum replacement of coarse RCA to 20% in new structural RAC. In an attempt to recover the strength of RAC, surface treatments [28], removal of residual mortar [29] and other solutions [30–34] were proposed in the past. However, most of these solutions are relatively expensive and/or impractical to use at industrial scale [28, 35], and thus are a hindrance for the wider adoption of RAC in construction. Moreover, the inconsistency of experimental results (especially at high levels of aggregate replacement) and limited amount of data also makes standardisation difficult [13, 36, 37], and therefore more experimental data is still necessary.

The hot and humid weather of Southeast Asia quickly corrodes the internal steel bars of reinforced concrete (RC) structures. This is particularly true in RC slatted slabs of livestock farms

(**Fig. 1**a) where waste/faeces are cleaned up daily with pressurised water (**Fig. 1**b), thus reducing the service life of such slabs to less than 10 years. This is a major issue for farmers, who face huge expenses due to the regular replacement of corroded slabs, as well as financial losses due to business interruption while the slabs are being replaced. Internal Fibre Reinforced Polymer (FRP) bars have proven to be a feasible option to prevent corrosion issues and to extend the service life of RC structures [38]. However, to date there is limited research on precast slatted slabs made with 100% RCA replacement [13, 35- 37,39].

(a) Damage and corrosion of slab (b) Daily cleaning with pressurised water

Fig. 1. Conventional steel RC concrete slatted labs in typical livestock shelter [39].

Overall deformation in FRP RC beams subjected to flexure consist of the flexural, shear and rigid body components. Shear induced deformations are normally negligible at service load and are usually ignored when calculating the total deflection of FRP RC members. However, previous research indicates that the component of shear induced deflection can be larger when FRP materials are used as reinforcement [40], and the amount of shear deformations can increase rapidly after the development of diagonal cracks, thus reducing considerably the overall stiffness of the thin concrete element [41-42]. Although the applications of fibre-reinforced polymer have been successfully used as both internally reinforced concrete elements as well as externally bonded RC elements as strengthening intervention techniques i.e. [43-45], serviceability criteria (crack widths and deflections) often control the design of FRP RC slabs. In RC slabs, most of the deflections at service load are due to flexural deformations. whereas shear deflections are relatively small and therefore they are neglected in the calculations. However, shear deflections can be significant once diagonal shear cracks develop. Previous work by Imjai et al. [46] showed that, after the service load level, additional deflections due to shear cracking in FRP RC elements can be up to 30% of the overall deflections. Imjai et al. proposed a simple (yet accurate) model to calculate such additional shear crack-induced deflections. However, the model needs to be verified against further experimental data, including elements cast with RAC. Moreover, only a few studies exist on the flexural behaviour of FRP RAC elements [47].

This article investigates experimentally and analytically the flexural behaviour of precast slatted slabs made with RAC. To achieve this, fifteen slabs are tested under four-point bending. Partial (50%) and total (100%) replacement of NA with RCA are investigated. To extend the service life of the slabs, nine of the slabs are reinforced with internal Glass FRP (GFRP) bars. The results are compared against crack widths and deflection predictions given by current design guidelines. Nonlinear finite element analysis (FEA) provides further insight into the behaviour of the FRP RAC slabs. This study contributes towards the development of new more sustainable structural solutions for FRP RAC elements, as well as towards more accurate models to calculate their deflections.

2. Experimental programme

The main parameters investigated in the tests included the amount of RCA replacing NA and the type of flexural bars (steel or GFRP), as well as the reinforcement ratio. The fifteen slabs were divided into three Series: 1) Series NC, cast with a NA concrete, 2) Series 50RAC, cast with a mix where 50% of the NA was replaced with RCA, and 3) Series 100RAC, cast with a mix where 100% of the NA was replaced with RCA.

2.1 Slab geometry and reinforcement

The slabs had a rectangular cross-section of 600×50 mm (width×depth) and a total length of 1050 mm, as shown in **Fig. 2**a. A maximum practical live load of 4.0 kN/m^2 was chosen in the design, which is typically used in the design of pigsty floors in Southeast Asia. Each test Series had five slabs: two slabs reinforced with ten longitudinal steel bars (diameters ϕ6 and ϕ9 mm), and three slabs reinforced with ten GFRP bars (diameters ϕ4, ϕ6 and ϕ9 mm). This led to over-reinforced flexural reinforcement ratios in all slabs (see **Table 1**), except slabs with GFRP bars of ϕ4 mm which were (slightly) under-reinforced and thus they were expected to fail by FRP rupture.

Comparatively, the balanced reinforcement ratio according to ACI 440.1R [48] was ρ_b = 1.33%. Three bars (ϕ6 mm) were also provided in the short direction of the slabs (**Fig. 2**a). The slabs had no reinforcement in the compression zone to minimise costs. It should be noted that the selected bars are the smallest commercial diameters available in Thailand. **Table 1** summarises the characteristics of the slabs and the corresponding parameters examined in this study. In this table, the first letter and number of the ID refer to the type (S=steel, F=GFRP) and diameter of bars (ϕ4, ϕ6 or ϕ9 mm). The numbers and letters after the hyphen refer to type of concrete (NC or RAC) and, if applicable, to the percentage of RCA replacement (50% or 100%). For example, F6-50RAC designates an FRP-reinforced specimen with ϕ6 mm bars cast with RAC at a 50% replacement level.

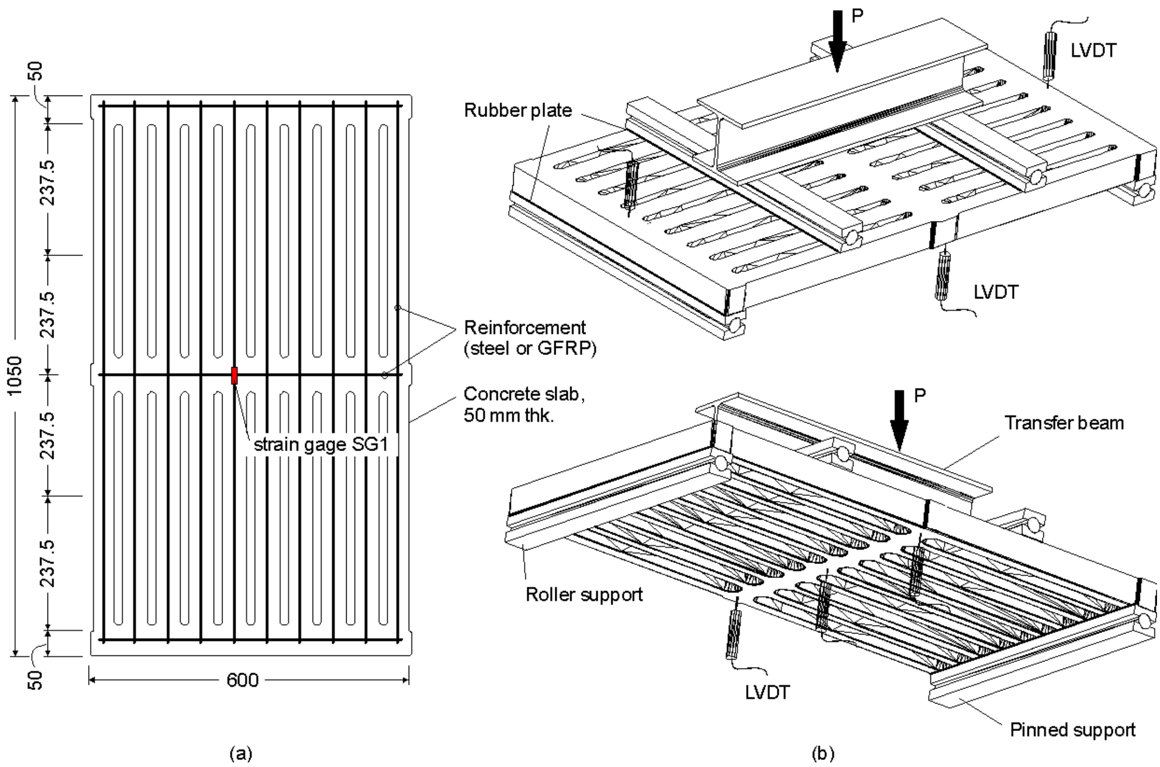

Fig. 2. Typical a) plan view and reinforcement details of slabs, and b) 3D view of test setup and instrumentation from top and bottom of slabs.

Table 1. Details of precast slabs tested in this study.

Slab ID	Type of concrete	Flexural reinforcement		
		Bars & area (mm^2)	ρ_f (%)	Type of bar
S6-NC	Series NC - Natural aggregate concrete	10ϕ6 = 282.7	2.89	Steel
S9-NC		10ϕ9 = 636.2	6.49	Steel
F4-NC		10ϕ4 = 125.7	1.28	GFRP
F6-NC		10ϕ6 = 282.7	2.89	GFRP

F9-NC		10ϕ9 = 636.2	6.49	GFRP
S6-50RAC	Series 50RAC -Recycled aggregate concrete 50% replacement	10ϕ6 = 282.7	2.89	Steel
S9-50RAC		10ϕ9 = 636.2	6.49	Steel
F4-50RAC		10ϕ4 = 125.7	1.28	GFRP
F6-50RAC		10ϕ6 = 282.7	2.89	GFRP
F9-50RAC		10ϕ9 = 636.2	6.49	GFRP
S6-100RAC	Series 100RAC - Recycled aggregate concrete 100% replacement	10-ϕ6 = 282.7	2.89	Steel
S9-100RAC		10ϕ9 = 636.2	6.49	Steel
F4-100RAC		10ϕ4 = 125.7	1.28	GFRP
F6-100RAC		10ϕ6 = 282.7	2.89	GFRP
F9-100RAC		10ϕ9 = 636.2	6.49	GFRP

2.2 Material properties

2.2.1 Flexural bars

All slabs with an "F" in their ID were reinforced with thermoset GFRP bars made of an epoxy matrix and continuous unidirectional glass fibres (65% by volume). The GFRP bars had a rough surface produced by peel ply. **Table 2** lists the average mechanical properties of the GFRP bars obtained from six bar coupons tested in direct tension. **Table 2** also reports the yield stress and ultimate stress of the steel bars.

Table 2. Mechanical properties of bars used in the slabs.

Type of bar	Nominal diameter (mm)	Modulus of elasticity (GPa)	Ultimate tensile stress (MPa)	Ultimate strain (%)
GFRP	ϕ4	46.2	890	1.9
	ϕ6	45.6	850	1.8
	ϕ9	45.6	750	1.7
Steel	ϕ6	210	(260*) 420	28
	ϕ9	210	(255*) 405	21

Note: *Average yield stress.

2.2.2 Concrete mixes

Ordinary Portland Cement (OPC) type I was used to cast the slabs. The RCA replaced both coarse and fine NA at levels of 50% (Series 50RAC) and 100% (Series 100RAC). The RCA was sourced from 150×300 mm concrete cylinders tested during the construction of a local structure. The original average compressive strength of the cylinders was 45 MPa. The cylinders were crushed to aggregate sizes of 9 mm (RCA#1) and 12 mm (RCA#2), as shown in **Fig. 3**a. These sizes matched the original size distribution of the NA, as shown in **Fig. 3**b. Fine RCA (RCA-FA) was also sieved and collected in a tray under the crushing machine. **Table 3** summarises the physical and mechanical properties of all aggregates.

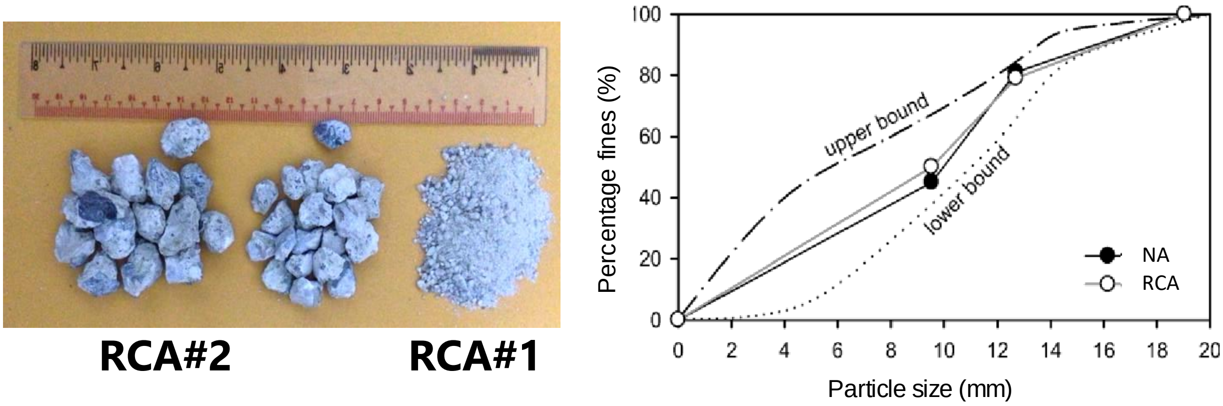

(a) (b)

Fig. 3. (a) View of coarse and fine recycled concrete aggregate (RCA), (b) particle size distribution of natural aggregate (NA) and RCA.

Table 3. Physical and mechanical properties of aggregates.

Properties	Coarse aggregates			Fine aggregates	
	CA	**RCA#2**	**RCA#1**	**FA**	**RCA-FA**
Bulk specific gravity (SSD)	2.71	2.43	2.51	2.60	2.77
Unit weight (kg/m^3)	1730	1397	1425	1550	1400
Water absorption (%)	0.28	4.59	5.13	1.05	2.65
Moisture (%)	0.61	2.24	2.14	1.35	2.42
Fineness modulus	-	-	-	2.7	1.8
Max. size (mm)	19.1	18.6	9.8	4.76	4.70
Impact value (%)	10.15	13.4	12.5	-	-
Crushing value (%)	21.77	23.12	20.12	-	-
Residual mortar (%)	-	32.5	30.2	-	32.5

Table 4 summarises the three mix designs used to cast the slabs. The mixes were designed according to ACI 211.1 [49] using a water/cement ratio of 0.53. The target compressive strength was 40 MPa and the target slump was 90 mm. 5 litres of superplasticiser (SP) were added to increase the workability of both NC and RAC mixes. An additional 5 kg of silica fume was added to improve the workability of the RAC mixes. **Table 5** shows the mechanical properties and standard deviations of the NC, 50RAC and 100RAC mixes at 28 days. The mean compressive strength was

obtained from three 150 mm cubes and three 100×200 cylinders according to BS EN 12390-3 [50]. The indirect tensile splitting strength (f_{ct}) was determined from tests on six 100×200 mm cylinders, according to BS EN 12390-6 [51]. The flexural strength ($f_{ct,fl}$) was obtained from four-point bending tests on three 100×100×500 mm prisms according to BS EN 12390-5 [52]. The mean modulus of elasticity calculated according to Eurocode 2 [53] was E_{cm}=31.1, 29.9 and 28.8 GPa for the NC, 50RAC and 100RAC mixes, respectively. All cubes, cylinders and prisms were cast at the same time and cured together with the slabs until the day of testing.

Table 4. Concrete mix proportions (in kg/m^3) and slump test results

Mix Type	CEM I	CA	RCA coarse	FA	RCA-FA	Water+SP	Silica fume	Slump (mm)
NC	357	1069	-	719	-	195	-	90
50RAC	357	505	564	350	350	195	5	85
100RAC	357	-	864	-	840	195	5	80

Table 5. Mechanical properties of concrete mixes at 28 days.

	Cylinder compressive strength f_{cm} (MPa)		**Cube compressive strength $f_{c,cm}$ (MPa)**		**Tensile strength f_{ct} (MPa)**		**Flexural strength $f_{ct,fl}$ (MPa)**	
Mix type	Mean	SD	Mean	SD	Mean	SD	Mean	SD
NC	42.0	3.3	45.9	3.8	4.1	1.5	4.5	1.2
50RAC	39.5	4.4	42.3	4.8	3.3	1.5	3.5	1.7
100RAC	37.1	4.5	39.3	5.4	3.1	1.1	3.1	1.5

Fig. 4a shows a typical plan view of an F4-100RAC specimen during casting. During construction, the concrete was carefully cast while the moulds were being gently compacted using a vibrating table (**Fig. 4**b).

(a) (b)

Fig. 4. (a) Plan view of typical slab moulds and FRP bars, and (b) compaction of concrete during casting.

2.3 Test setup and instrumentation

The slabs were tested in four-point bending according to the schematic setup shown in **Fig. 2**b. The slabs were simply supported on pins and rollers located at 50 mm from the edge of the slab, which reflects typical installation practices in livestock farms. The free span was therefore 950 mm, whereas the shear span was 237.5 mm. The shear span to effective depth (effective depth = 35 mm) ratio *a*/*d* was equal to 6.7. Accordingly, the slabs were classified as Type II in Kani's shear valley and therefore the "beam action" was expected to be a combination of flexure and shear [54].

The load was applied using a 250 kN actuator in displacement control mode at a rate of 1.0 mm/min. A stiff transfer beam was used to transfer the load to the slabs. The deflections at the mid-span were measured using three Linear Variable Displacement Transducers (LVDTs) located at the bottom of the slabs (see **Fig. 2**b). Two additional LVDTs were also placed above the supports (on top of the slabs) to calculate net deflections. A strain-gauge (SG1) bonded onto the flexural steel or GFRP bars monitored the strains at the mid-span during testing (see **Fig. 2**a). At approximately every 1 kN, cracks were marked, and the width of selected cracks was measured using a handheld micrometre (accuracy = 0.002 mm). Eventually, all slabs were tested up to failure.

3. Results and discussion

3.1 Load-deflection curves and failure modes

Fig. 5a, b and c compare, respectively, the load–mid-span deflection curves of slabs NC, 50RAC and 100RAC. **Table 6** summarises the test results in terms of a) load at onset of flexural cracking P_{cr} and corresponding mid-span deflection Δ_{cr}, b) maximum load P_{max} and corresponding deflection Δ_{max}, c) failure mode, d) energy absorption ζ of the slabs, and e) measured crack widths. The maximum recorded load was considered as P_{max}. All tests were halted after a drop of 10-20% in P_{max}, once a clear failure mode was identified. The value ζ was calculated as a total area under the load-deflection curve up to a drop of 10% in P_{max}.

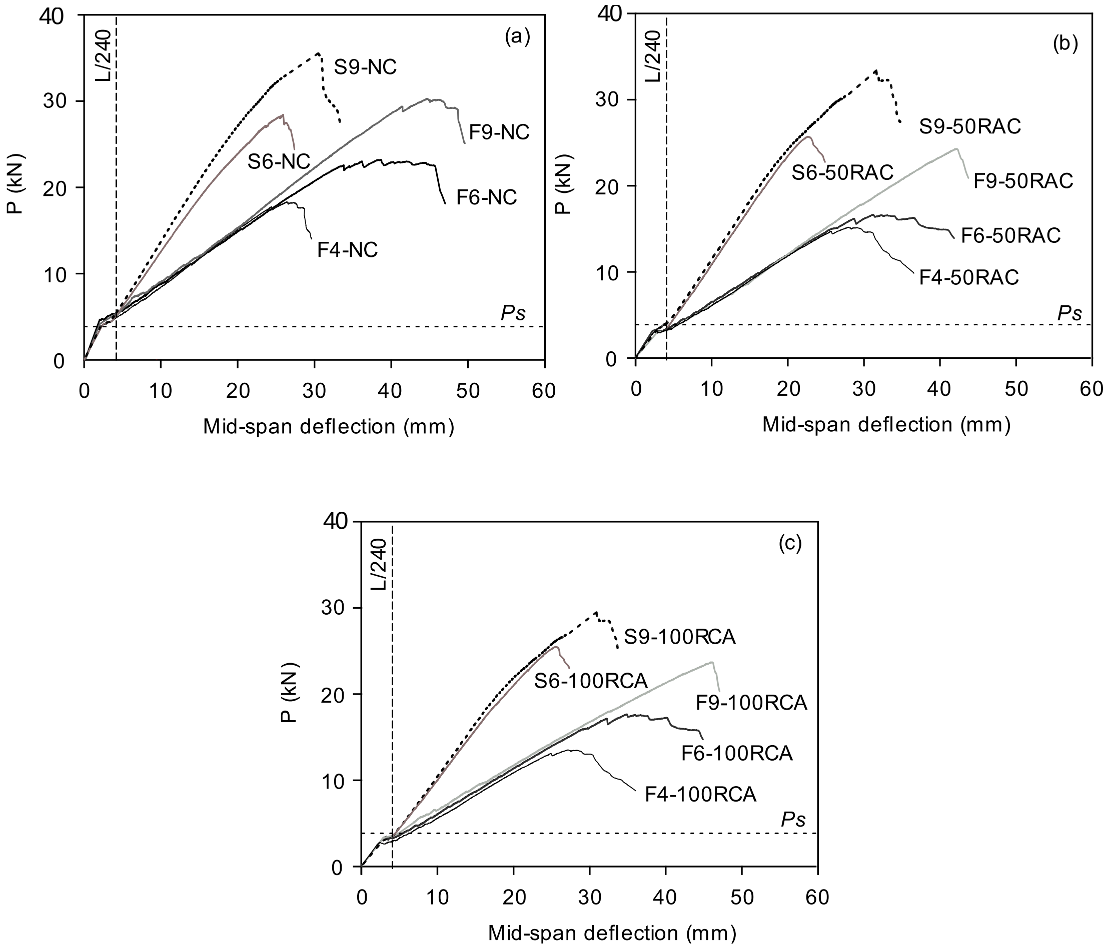

Fig. 5. Load-deflection curves of slabs (a) NC, (b) 50RAC, and (c) 100RAC.

As shown in **Fig. 5**a-c, all the slabs had a linear response until the onset of flexural cracking at P_{cr}. **Fig. 5**a and the data in **Table 6** show that the average P_{cr} of slabs NC (4.46 kN) was 12% higher than the cracking load at service condition P_s (or 4 kN/m^2). Conversely, **Fig. 5**b-c show that the average P_{cr} of slabs 50RAC (2.98 kN) and slabs 100RAC (3.12 kN) were below P_s, which indicates that flexural cracks developed before reaching such service load level. At load P_{cr}, slabs NC had an average mid-span deflection (2.98 mm) 8% higher than the average mid-span deflection of slabs 50RAC (2.72 mm), but 3% lower than the average of slabs 100RAC (3.04 mm). All slabs met the deflection limit of L/240 imposed by ACI 318 (see **Fig. 5**a-c).

Major flexural cracks were observed as the load increased. The stiffness of the load–deflection curve of slabs "F" reduced gradually when the strain in the longitudinal GFRP bars reached 4500-5000 με. Overall, the maximum capacity $P_{\max}$ of slabs "S" was higher than that of counterpart slabs "F". It was also found that the mid-span deflections $\Delta_{\max}$ of slabs "S" (see **Table 6**) were somehow similar, regardless of the type of concrete used to cast the slabs. For FRP-reinforced slabs with similar reinforcement ratios, the capacity P_{max} of RAC slabs was always lower than those of NC counterparts (up to 27% and 24% for 50% and 100% levels of RCA replacement, respectively). However, the use of RAC instead of normal aggregate concrete affected the mid-span deflections Δ_{max} only marginally, with such a value sometimes decreasing and others increasing. It should be noted that the variations of the ultimate load of concrete slabs with different RCA contents can be attributed to the natural variability of the RCA itself, as well as to the presence of residue mortar on the RCA. These aspects are known to deteriorate bond stresses between FRP and concrete, and therefore the ultimate performance of RAC elements.

Table 6. Summary of main results of tested slabs.

Series	ID	P_{cr} (kN)	Δ_{cr} (mm)	P_{max} (kN)	Δ_{max} (mm)	Failure mode [a]	ζ *(kN-mm)*	w_f @ P_s (mm)		S_{max} @ P_{max} (mm)	
								Test	*Predicted* [b]	*Test*	*Predicted* [b]
NC	S6-NC	4.6	2.9	28.6	26.1	CC	409	0.38	0.54	3.25	4.94
	S9-NC	4.8	3.0	35.5	30.9	CC	678	0.25	0.27	2.30	2.37
	F4-NC	4.1	3.1	18.1	26.2	BR	333	0.60	0.94	4.30	6.96
	F6-NC	4.3	3.0	23.1	38.5	CC	686	0.35	0.45	2.35	3.23
	F9-NC	4.5	2.9	30.1	45.8	CC	831	0.20	0.23	1.25	1.50
50RAC	S6-50RAC	3.1	2.4	25.9	23.0	CC	326	0.43	0.54	4.30	4.94
	S9-50RAC	3.0	2.3	33.2	31.7	CC	631	0.25	0.27	1.15	2.37
	F4-50RAC	3.1	3.0	15.2	29.3	BR	332	0.75	0.94	6.40	6.96
	F6-50RAC	2.9	3.0	16.8	33.1	CC	429	0.40	0.45	2.45	3.23
	F9-50RAC	2.8	2.9	24.2	42.1	CC	539	0.15	0.23	1.40	1.50
100RAC	S6-100RAC	3.2	3.0	25.6	25.9	CC	259	0.42	0.54	3.55	4.94
	S9-100RAC	3.3	2.9	29.8	31.0	CC	464	0.25	0.27	2.10	2.37
	F4-100RAC	3.0	3.2	13.8	27.9	BR	291	0.80	0.94	5.40	6.96
	F6-100RAC	3.0	3.1	17.8	36.2	CC	466	0.35	0.45	3.25	3.23
	F9-100RAC	3.1	3.0	23.9	46.7	CC	553	0.20	0.23	1.45	1.50

Notes: [a] BR=GFRP bar rupture, CC=concrete crushing. [b] Crack widths predicted by ACI 318 or ACI 440.1R (Eq. A.6).

As shown in **Table 6** and regardless of the type of concrete, all slabs “S” failed by concrete crushing (CC). As expected, the three under-reinforced slabs F4 failed due to bar rupture (BR) at bar strains of 1.0%-1.5%. Comparatively, (over-reinforced) slabs F6 and F9 failed due to concrete crushing (CC). The failure mode of all tested slabs was controlled by a combination of flexure and diagonal shear cracking. **Fig. 6** shows typical failures of RAC slabs, which are representative of the slabs tested in this study.

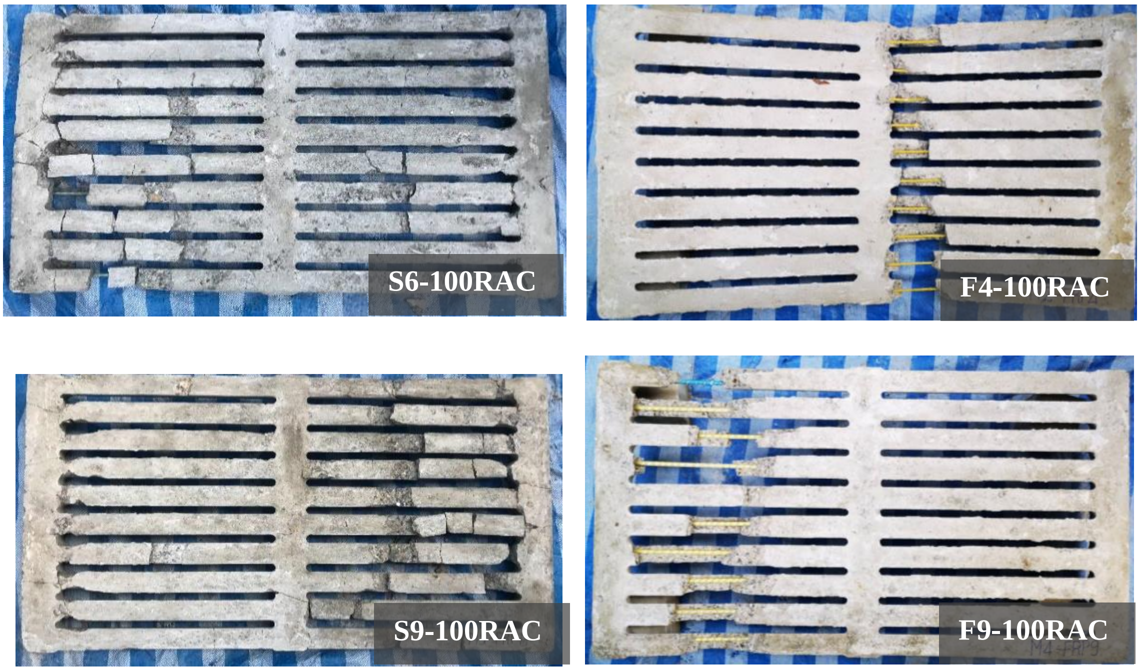

Fig. 6. Typical failure of tested slabs (Series 100RAC).

Table 6 also compares the energy absorption ζ of each slab. The energy absorption for NC specimens was generally higher than the counterpart RAC specimens with similar reinforcement ratio. The results also show that, for the same type of concrete, slabs “F” had higher energy absorption that the counterpart slabs “S” with similar reinforcement ratio (except slab F9-50RAC). In general, the energy absorption is small in slabs that failed due to bar rupture (BR).

3.2 Crack widths and crack spacing

Fig. 7a compares the (average) measured crack spacing at the constant moment zone of the slabs, and the maximum crack spacing S_{max} predicted by ACI 318 (slabs “S”) or ACI 440.1R (slabs “F”). The results show that, compared to the measured crack spacings of slabs “S”, the maximum crack spacings calculated by ACI 318 were conservative (22% on average). Moreover, the maximum crack spacings predicted by ACI 440.1R were also conservative (17% on average) for slabs "F" when compared to the experimental values. The closer crack spacing of slabs "S" can be attributed to the development of a more uniform (better) bond along the steel bar–concrete interface, when compared to the FRP bar–concrete interface of slabs "F". The results in **Fig. 7**a also confirm that the ACI approach predicts conservatively the crack spacing of the slatted slabs tested in this study.

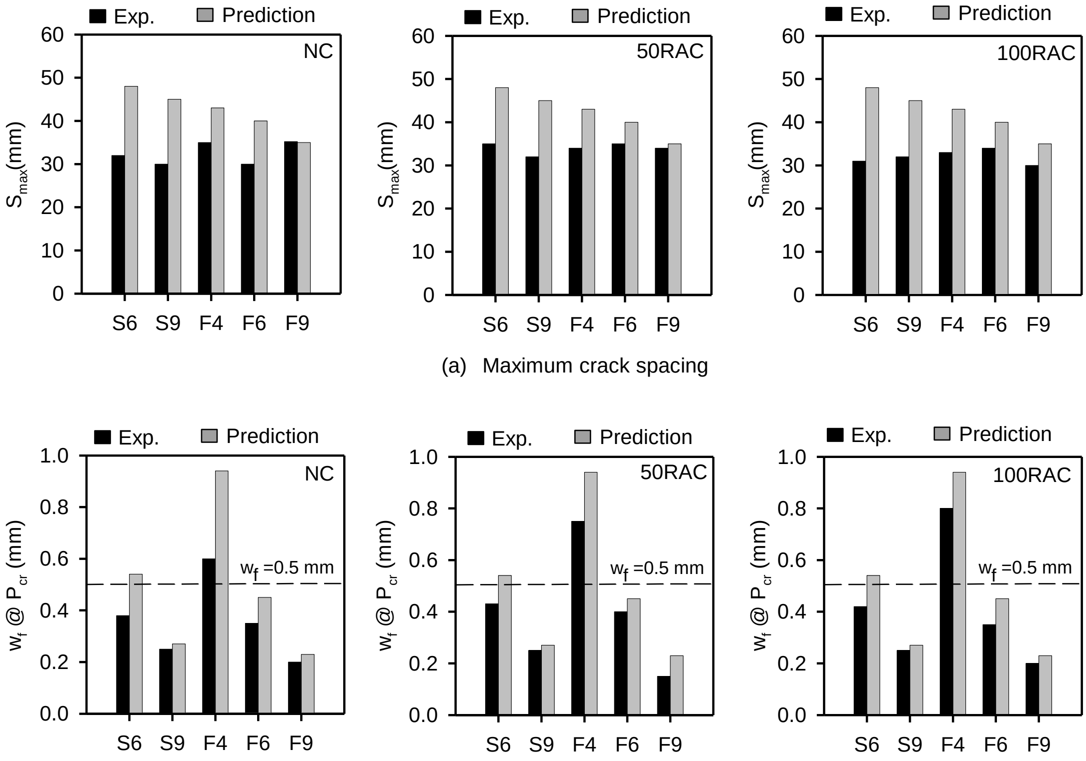

(a) Maximum crack spacing

(b) Crack widths at the end of pre-cracked stage

Fig. 7. Comparison of experimental and ACI predictions of (a) maximum (average) crack spacing and (b) crack width at P_{cr} at service load level.

Fig. 7b compares the measured crack width w_f at P_{cr} and the corresponding ACI 440.1R predictions. At P_{cr}, the measured crack width of slabs "S" (all series) was 0.25-0.43 mm, which is close to the predicted values. The measured crack widths of slabs F4 (0.60 mm for NC, 0.75 mm for 50RAC and 0.80 mm for 100RAC) were wider compared to the crack widths of slabs F6. At the service condition load P_s, the observed crack widths of specimens F4 were >0.5 mm and therefore above the serviceability crack width limits suggested in ACI 440.1R. This can be attributed to the fact that the ϕ4 mm GFRP bars were rather small and thus unable to provide a good bond between the bars and the concrete. On the other hand, for slabs F6 and F9 (with larger bar diameters), the observed crack widths were below 0.5 mm and therefore the slabs met the serviceability limits of ACI 440.1R. The results in **Fig. 7**b also indicate that, at the service load level of slabs "S", the crack widths calculated by ACI 318 were on average only 7% larger than the crack widths measured in the tests. For Series NC, 50RAC, 100RAC, the crack widths at maximum load calculated by ACI 440.1R were conservatively 15%, 12% and 10% higher than the measured crack, respectively.

The results in this section confirm that ACI 440.1R predicts conservatively the crack widths of the FRP-reinforced RAC slabs at service load (within 7%) and maximum load (within 25%). However, further tests and analyses with different recycled aggregate concretes are necessary to fully validate this observation. This is particularly true because the actual characteristics of the cracks rely heavily (among others) on concrete properties such as the compressive strength, as well as the bond stress mobilised between the FRP bars and surrounding concrete.

4. Analysis of FRP RC slab deflections

4.1. Flexural deflections

To calculate flexural short-term deflections of FRP RC elements, ACI 440.1R [48] adopts an effective moment of inertia I_e, as defined by Eq. (1):

$$I_e = \frac{I_{cr}}{1-\gamma\left(\frac{M_{cr}}{M_a}\right)^2\left(1-\frac{I_{cr}}{I_g}\right)} \tag{1}$$

where I_g and I_{cr} are the gross and cracked moments of inertia, respectively; and M_{cr} and M_a are the cracking and applied flexural moment, respectively. The factor γ in Eq. (1) depends on the load and boundary conditions, which implicitly accounts for the length of the member's uncracked areas. A value γ=1.72-0.72(M_{cr}/M_a) is recommended for FRP RC members [55,56].

Eurocode 2 [53] includes the effect of tension stiffening and proposes Eq. 2 to calculate the short-term deflection due to flexure of FRP RC members:

$$\Delta = \beta \left(\frac{M_{cr}}{M_a}\right)^2 \Delta_g + \left[1 - \beta \left(\frac{M_{cr}}{M_a}\right)^2\right] \Delta_{cr} \tag{2}$$

where Δ_g and Δ_{cr} are the uncracked and cracked-state deflections, respectively; β is a duration or repetition load factor; and the rest of the variables are as defined before. For concrete elements reinforced with GFRP bars, a value β=0.5 is recommended [57].

4.2. Shear crack-induced deflections

The authors have proposed a novel model to account for the additional shear crack-induced deflections in GFRP RC elements [46]. The model assumes that idealised shear cracks form within the shear span a of an element, as shown in **Fig. 8**a. Accordingly, the additional shear crack-induced deflection can be calculated using Eq. (3):

$$\Delta_{sc} = \sum \left[\frac{w_i \cdot Sin\theta_i}{y_i}\right] \cdot \left[\frac{L/2}{1 + (l_1/l_2)}\right] \tag{3}$$

where w_i is the width of the shear cracks; θ_i is the inclination angle of the shear cracks; y_i is the height of the crack tips; and L is the total span of the flexural member ($L=l_1+l_2$).

In reality, the locations of actual shear crack tips are unknown, which in turn makes measuring their location difficult. As a result, Eq. (3) was simplified by assuming that the tip of a single fictitious shear crack of width w_s (where w_s is the sum of all the shear crack widths) is located very close to the loading point within the shear span a, as illustrated in **Fig. 8**c. This in turn defines the horizontal distances from the individual crack tip to the support l_1 and l_2. Therefore, the horizontal distance l_2 can be defined as approximately equal to the shear span a. By assuming θ=45° and y=0.9h (h=element depth), Eq. (3) can be re-written as:

$$\Delta_{sc} = 0.393 w_s \left(\frac{a}{h}\right) \tag{4}$$

In this study, Eq. (4) was used to calculate the additional shear crack-induced deflections of the tested slabs. Note that the results from Eq. (4) have to be added to the flexural deflections to calculate the total deflection of the slabs.

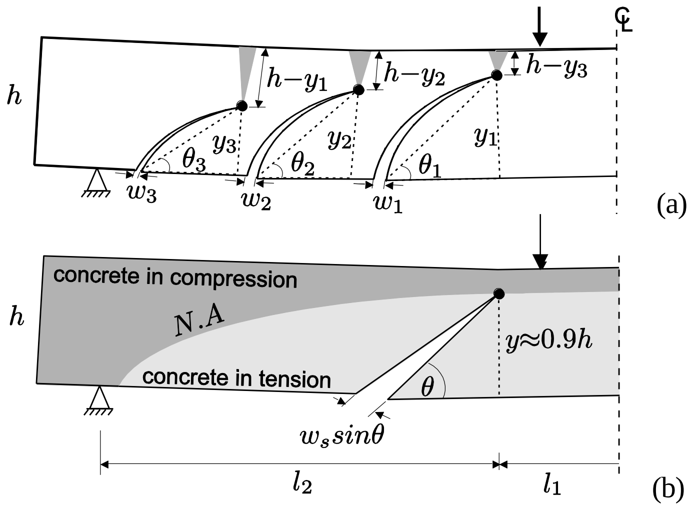

Fig. 8. Shear crack-induced deflection model by Imjai et al. [46].

4.3. FEA predictions

To provide further insight into deflections, slabs “F” were modelled using Abaqus® software [58]. The analyses were performed with the inclusion of both material and geometric nonlinearities. The concrete of all slabs was modelled using C3D10M tetrahedron elements (see **Fig. 9**) with a modified second-order integration scheme. In this study, the robust Abaqus FE software offered the optimization mesh sensitivity topology for the curve and irregular zone. This is automatically implemented by the software to minimize the error due to distortion of the irregularity FEM during the analysis.

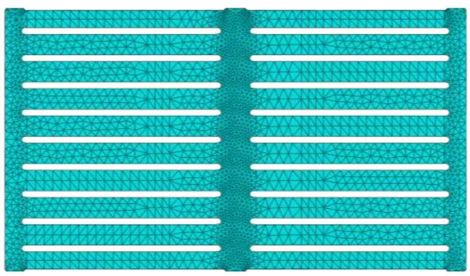

Fig. 9. 3D tetrahedron meshing in FE model.

The material properties were taken from the laboratory test results listed in **Table 2**. A concrete damaged plasticity (CDP) model was adopted in the analyses, which is extensively used in the analysis of RC structures [59,60]. Accordingly, the constitutive uniaxial compressive behaviour was linear up to the initial yield point, σ_{c0}, as shown in **Fig. 10**a. Afterwards, the plastic zone is represented by stress hardening up to the ultimate stress σ_{cu}, followed by strain softening beyond the ultimate stress. Under uniaxial tension, the stress-strain relationship is linear-elastic up to the failure stress $\sigma_{t0,}$ which corresponds to the initiation of micro-cracking (**Fig. 10**b). Beyond the failure stress, the formation of cracks in the tensioned zone is represented by a softening stress-strain response, which induces strain localisation (‘jumps’) in the concrete structure. The recycled concrete was defined using the CDP model by Liu and Chen [61].

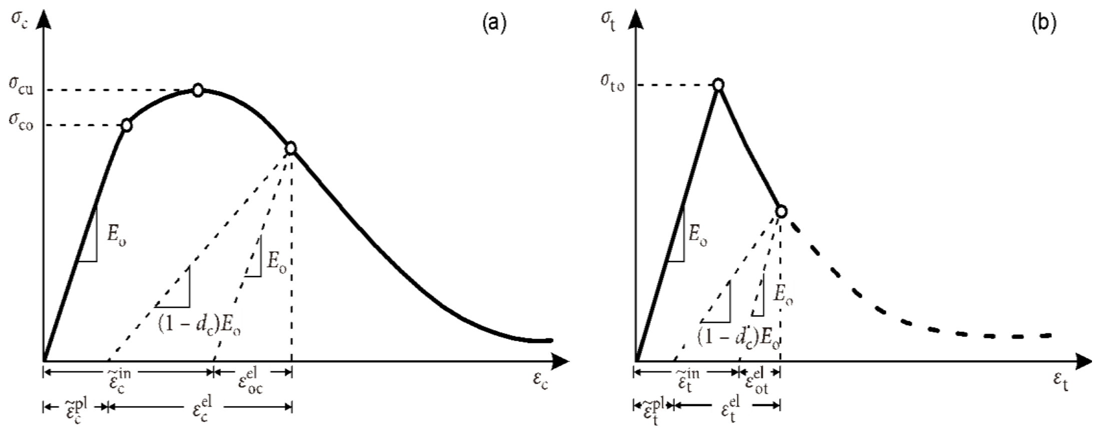

Fig. 10. Constitutive models of recycled concrete materials for FE analyses (a) uniaxial compression, (b) softening diagram in tension

The compressive stress-strain relationship was calculated using the *fib* Model Code 2010 [62]. To take into account its dependency on the specimen geometry and ensuring almost mesh-independent simulation results, the descending branch in **Fig. 10**a was obtained using the formulation proposed by Kratzig & Polling [63]. Likewise, the nonlinear descending branch of the tensile stress-strain relationship in **Fig. 10**b was derived from the stress-crack opening relationship proposed by Hordijk [64]. The compressive damage parameter D_c is as the ratio between the inelastic strain and total strain shown in **Fig. 10**a. Similarly, the tensile damage parameter D_t in Abaqus® is defined as the ratio of the cracking strain to the total strain (**Fig. 10**b). If damage parameters are not specified, the model behaves as a plasticity model. In this study, an exponential function was used to calculate do damage variable for both compression and tension behaviour.

The densities and Young's moduli obtained from the tests were assigned to the FE model. The additional flow potential, yield surface, and viscosity parameters for the concrete damaged plasticity material model were: dilation angle=40 degrees, eccentricity=0.1; f_{b0}/f_{c0}=1.17, and K=2/3 were adopted and used in this study. Since concrete exhibits softening behaviour and stiffness degradation that often led to severe convergence difficulties, a viscoplastic regularization technique was added to the CDP model to permit stresses to be outside of the yield surface by using a viscosity parameter μ=0.001.

The GFRP bars were simulated using 2-node truss (T3D2) embedded elements with two Gauss-Legendre integration points. A linear stress-strain relationship was adopted for the GFRP bars. Since the main focus of the analysis was to examine the deflection of the slabs during service, perfect bond was assumed between the bars and the surrounding concrete. This was reasonable because there was no evidence of bond failures in the tested slabs. In many precast concrete elements however, bond-slip of the reinforcement can play an important role in the response, especially at high levels of load or after yielding of the steel reinforcement.

The supports of the experimental set-up were modelled using elastic C3D10M tetrahedron elements. The boundary conditions and loads were applied directly on the supports to avoid unrealistic stress fields in the slabs. The load was applied by direct displacement-control at the mid-span of the slab. To model the concrete slab, the element size was optimised and varied where the irregular geometry was detected. Fig. 11 shows a typical slab at failure. Overall, the predicted cracking patterns and concrete damage agree well with the experimental observations. The negative plastic strains shown in the figure are due to the support restrain conditions as the slabs were supported by the flat steel frame with a bearing area of 50 mm, which in turn reflects how the slabs are installed in real applications.

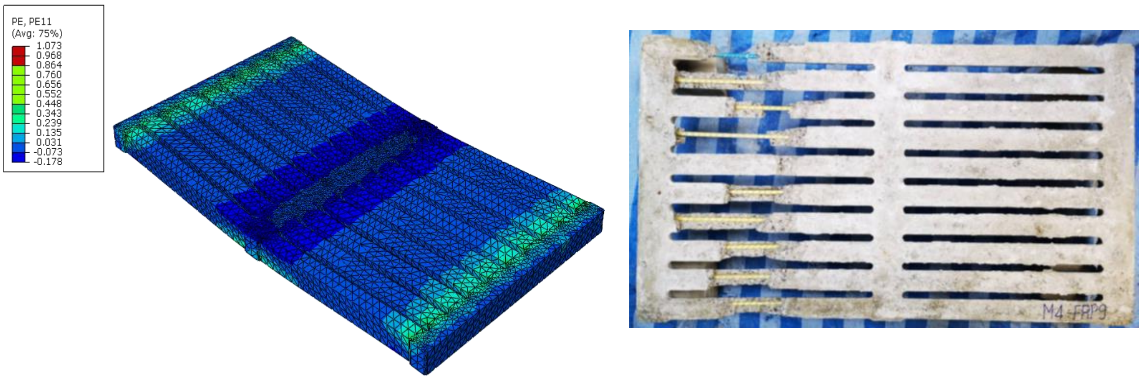

Fig. 11. Maximum positive principal plastic strains of F9-100RAC slab and specimen at failure.

4.4. Comparison of deflections of FRP RC slabs

In this study, the numerical analysis was terminated a pre-defined number of steps and the analysis results were adequate to compare the deformations of the experiments at the serviceability level as this is of interested in SLS deflection and compared to the experiments and code predictions. **Fig. 12**a-i compare the load-deflection curves obtained from the tests and those calculated using the: a) ACI 440.1R approach (i.e. Eq. (1)), b) Eurocode 2 approach (i.e. Eq. (2)), c) Eurocode 2 approach plus the shear crack-induced deflections (i.e. Eq. (2) + Eq. (4)), and c) finite element analysis. It is also observed that, at diagonal cracking load level, the deflections of slabs 50RAC and 100RAC are (on average) 23% higher than those of slabs NC. This can be attributed to the softer bond between FRP bars and RAC [65], which led to wider cracks and thus larger deflections when compared to NC slabs. However, the deflections at P_{max} of counterpart slabs showed no clear increasing or decreasing trend. This confirms that, for the slabs tested in this study, the use of RAC had a minor effect on the deflections at maximum load. The results show that, for FRP-reinforced RAC slabs, the analytical and FEA results match well the experimental results before the onset of diagonal shear cracking. However, after diagonal cracking occurs, the ACI 440.1R approach tends to underestimate the deflections by up to 10%. At P_{max}, the ACI 440.1R and EC2 approaches underestimate the deflections by up to 30% and 12%, respectively. **Table 7** also compares the deflections of slabs "F" at the onset of diagonal shear cracking and at P_{max} along with the corresponding analytical and FEA predictions. The table also include the Experimental/Prediction ratios (Exp./Pre.) and standard deviations (SD). The results in **Table 7** show that the deflections calculated according to Eurocode 2 plus the shear crack-induced deflection (i.e. Eq. (2) + Eq. (4)) match better the test results both at diagonal cracking load (Exp./Pre.=1.01, SD=0.03) and at maximum load P_{max} (Exp./Pre=1.07, SD=0.03). This indicates that the additional component of deflection is due to the development of shear cracking.

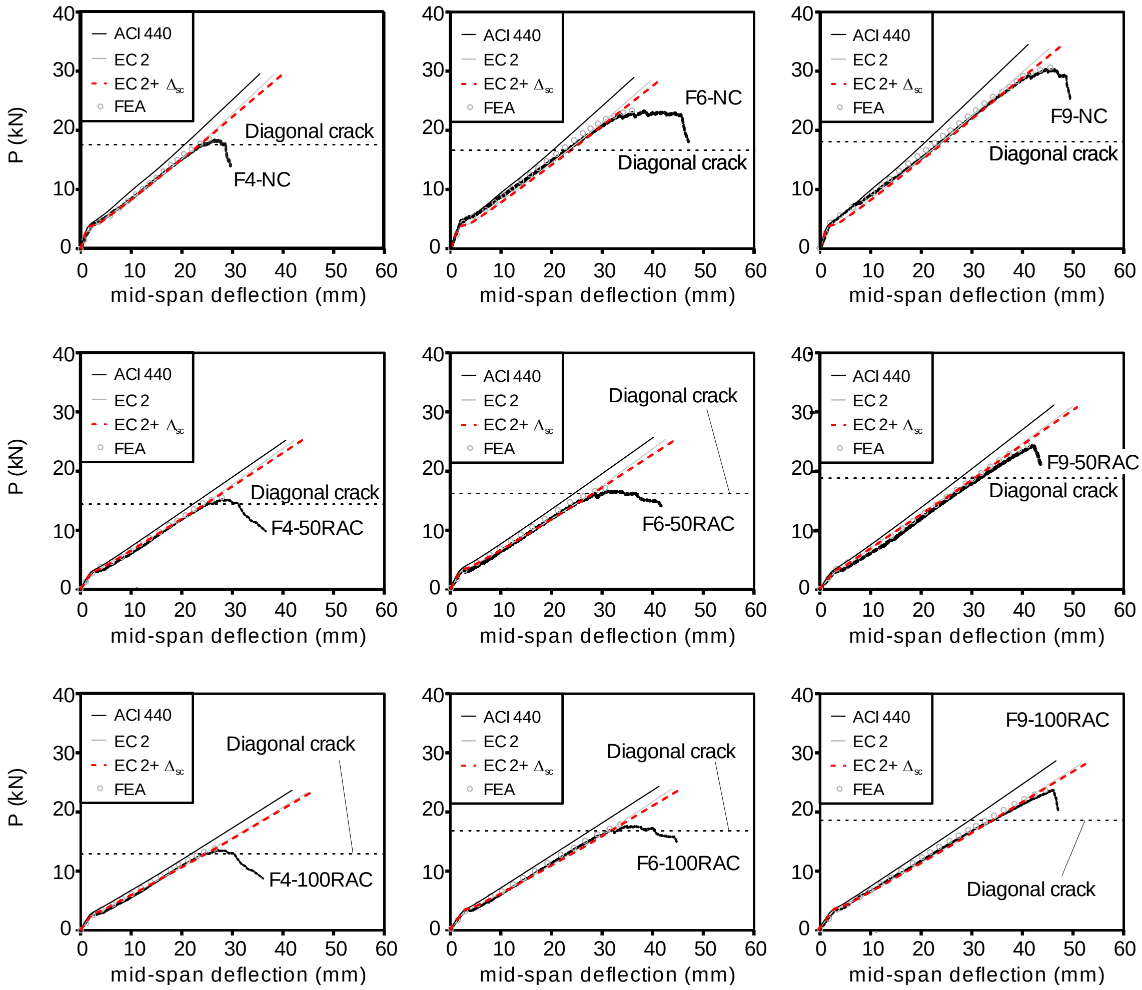

Fig. 12. Experimental vs FE predicted load-deflection curves of tested slabs.

The results in **Fig. 12**a-i and **Table 7** also show that the Concrete Damage Plasticity (CDP) model adopted in the FEA was affective at predicting the deflection of the slabs. After diagonal shear cracks formed, the deflections from the FEA were always lower than the measured deflections. However, the differences were always less than 5% (except for F4-NC) as confirmed by a Exp./Pre=1.03 and a SD=0.02. After diagonal cracking occurs, the FE predictions tend to underestimate the deflections of slabs "NC" (e.g. F6-NC and F9-NC). The FE predictions were expected to be stiffer than the experimental values since the additional deflections due to rigid crack opening were not considered in the analysis. Based on these results, it is evident that the FE predictions tend to underestimate deflections after major cracks form in the element (at P_{max}, Exp./Pre=1.05 and a SD=0.04). This can be attributed to an overall underestimation of deformation due to several cracks opening simultaneously (such as shear cracks), an effect that is more pronounced after the onset of diagonal cracking as reported previously [59]. Based on these results, it can be concluded that CDP is an appropriate modelling approach to predict the deformations of RAC slabs reinforced with FRP bars reasonably well up to the maximum load level, especially for flexural-dominated concrete members such as slabs. It should be noted that, in the case of shear-dominated members (e.g. deep concrete beams), shear crack-induced deflections are expected to contribute more to the overall deformation of RAC elements. In this case, shear crack-induced deflections should always be considered in the serviceability limit state design. However, further analysis of structures with other types of RAC should be investigated to confirm the findings presented in this study.

Table 7. Comparison of experiment and calculated deflections of tested slabs.

Series	Specimen ID	Δ_{mid} at diagonal cracking (mm)					Δ_{mid} at P_{max} (mm)				
		Exp.	**ACI 440.1R**	**EC2**	**EC2 + Δ_{sc}**	**FEA**	**Exp.**	**ACI 440.1R**	**EC2**	**EC2 + Δ_{sc}**	**FEA**
NC	F4-NC	24.5	20.8	24.5	25.3	25.1	26.2	20.9	25.3	25.9	26.0
	F6-NC	23.2	21.8	23.5	23.8	22.5	38.5	28.5	33.7	34.8	37.5
	F9-NC	24.7	21.6	23.1	23.5	23.5	45.8	38.6	41.2	42.6	45.8
50RAC	F4-50RAC	26.1	21.8	25.2	25.5	24.9	29.3	24.6	26.5	26.8	29.0
	F6-50RAC	28.9	24.5	28.4	28.5	28.6	33.1	26.5	29.1	30.2	32.5
	F9-50RAC	32.1	27.2	31.1	31.5	31.6	42.1	37.2	39.5	40.2	41.5
100RAC	F4-100RAC	25	21.9	24.6	25.1	24.5	27.9	22.4	25.4	25.8	27.9
	F6-100RAC	32.5	27.2	31	31.4	31.1	36.2	30.1	34.5	34.8	35.0
	F9-100RAC	34.7	31.2	34.4	34.5	33.5	46.7	39.4	44.8	45.1	46.1
Average Exp./ Pre.		-	*1.15*	*1.02*	*1.01*	*1.03*	-	*1.22*	*1.09*	*1.07*	*1.05*
	SD	-	*0.04*	*0.03*	*0.03*	*0.02*	-	*0.06*	*0.04*	*0.03*	*0.04*

5. Conclusions

This article investigated experimentally and numerically the serviceability behaviour of FRP-reinforced slatted slabs cast with recycled aggregate concrete (RAC). Fifteen slabs are tested in three Series: a) Series NC cast with natural aggregate concrete, b) Series 50RAC cast with a concrete made with 50% recycled concrete aggregate, and c) Series 100RAC cast with a concrete made with 100% recycled concrete aggregate. Finite Element Analyses (FEA) provided further insight into the deflections of the slabs. Based on the results of this study, the following conclusions can be drawn:

- Overall, for FRP-reinforced slabs with similar reinforcement ratios, the maximum capacity of RAC slabs was always lower than that of counterpart slabs with natural aggregate concrete (up to 27% and 24% for 50% and 100% levels of natural aggregate replacement, respectively). However, the use of RAC instead of normal aggregate concrete affected the mid-span deflections at maximum load P_{max} only marginally, with such a value sometimes increasing and others decreasing.
- For the FRP-reinforced RAC slabs tested in this study, ACI 440.1R predicted conservatively the crack widths of at service load (within 7%) and maximum load P_{max} (within 25%).
- The results show that, for FRP RAC slabs, the analytical and Finite Element Analysis results matched well the experimental results before the onset of diagonal shear cracking. However, after diagonal shear cracking occurs, the ACI 440.1R approach underestimated the deflections by up to 10%. At maximum load P_{max}, the ACI 440.1R and Eurocode 2 approaches underestimated the experimental deflections by up to 30% and 12%, respectively.
- For the RAC slabs tested in this study, the addition of shear crack-induced deflections (calculated with a novel model proposed by the authors) to the flexural deflections given by Eurocode 2 led to more accurate predictions of deflections at both diagonal cracking load

(Exp./Pre.=1.01, SD=0.03) and at maximum load P_{max} (Exp./Pre=1.07, SD=0.03). It is therefore suggested that shear crack-induced deflections are always considered when calculating the deflections of RAC elements where shear cracking occurs.

- The Concrete Damage Plasticity approach adopted in the FEA was suitable to predict the deformations of FRP-reinforced RAC slabs reasonably well up to the maximum load. However, further research is necessary to validate this observation.

Acknowledgements

This research was funded by National Research Council of Thailand (NRCT5-RSA63019-04). The authors acknowledge the support provided by the Capacity Enhancement and Driving Strategies for Bilateral and Multilateral Cooperation for 2021 (Thailand and UK).

References

References

[1] Etxeberria, M., Marí, A. R., & Vázquez, E. (2007). Recycled aggregate concrete as structural material. *Materials and Structures, 40*(5), 529-541. doi:10.1617/s11527-006-9161-5

[2] Hole, M. D. S. (2013). *Used concrete recycled as aggregate for new concrete.* MEng dissertation, Universitat Politècnica de València, Spain.

[3] Katiyar, M., & Singh, S. (2019). Concrete with Alternative Aggregates -Green Concrete, *IRJET Journal*, 6(8), 520-524.

[4] Putri, A.D. (2017). Recycled concrete aggregate (RCA) for the use in construction: General review. Advance Concrete Materials, School of Civil Engineering, Beijing Jiaotong University, 1-14

[5] Collins, F. (2010). Inclusion of carbonation during the life cycle of built and recycled concrete: Influence on their carbon footprint. *The International Journal of Life Cycle Assessment, 15*, 549-556. doi:10.1007/s11367-010-0191-4

[6] Jiménez, L. F., Domínguez, J., & Vega-Azamar, R. (2018). Carbon Footprint of Recycled Aggregate Concrete. *Advances in Civil Engineering, 2018*, 1-6. doi:10.1155/2018/7949741

[7] Bostanci, S. C., Limbachiya, M., & Kew, H. (2018). Use of recycled aggregates for low carbon and cost effective concrete construction. *Journal of Cleaner Production, 189*, 176-196. doi:https://doi.org/10.1016/j.jclepro.2018.04.090

[8] Xiao, J., Wang, C., Ding, T., & Akbarnezhad, A. (2018). A recycled aggregate concrete high-rise building: Structural performance and embodied carbon footprint. *Journal of Cleaner Production, 199*, 868-881. doi:https://doi.org/10.1016/j.jclepro.2018.07.210

[9] Tam, V. W. Y., Soomro, M., & Evangelista, A. C. J. (2018). A review of recycled aggregate in concrete applications (2000–2017). *Construction and Building Materials, 172*, 272-292. doi:https://doi.org/10.1016/j.conbuildmat.2018.03.240

[10] Maduabuchukwu Nwakaire, C., Poh Yap, S., Chuen Onn, C., Wah Yuen, C., & Adebayo Ibrahim, H. (2020). Utilisation of recycled concrete aggregates for sustainable highway pavement applications; a review. *Construction and Building Materials, 235*, 117444. doi:https://doi.org/10.1016/j.conbuildmat.2019.117444

[11] Xu, X., Luo, Y., Sreeram, A., Wu, Q., Chen, G., Cheng, S., et al. (2022). Potential use of recycled concrete aggregate (RCA) for sustainable asphalt pavements of the future: A state-of-the-art review. *Journal of Cleaner Production, 344,* 130893. doi:https://doi.org/10.1016/j.jclepro.2022.130893

[12] Kisku, N., Joshi, H., Ansari, M., Panda, S. K., Nayak, S., & Dutta, S. C. (2017). A critical review and assessment for usage of recycled aggregate as sustainable construction

material. *Construction and Building Materials, 131*, 721-740. doi:https://doi.org/10.1016/j.conbuildmat.2016.11.029

[13] Setkit, M., Leelatanon, S., Imjai, T., Garcia, R., & Limkatanyu, S. (2021). Prediction of Shear Strength of Reinforced Recycled Aggregate Concrete Beams without Stirrups. *Buildings, 11*(9), 402. https://www.mdpi.com/2075-5309/11/9/402

[14] Butler, L. (2012). *Evaluation of Recycled Concrete Aggregate Performance in Structural Concrete.* UWSpace, http://hdl.handle.net/10012/6737

[15] Wagih, A. M., El-Karmoty, H. Z., Ebid, M., & Okba, S. H. (2013). Recycled construction and demolition concrete waste as aggregate for structural concrete. *HBRC Journal, 9*(3), 193-200. doi:https://doi.org/10.1016/j.hbrcj.2013.08.007

[16] Malešev, M., Radonjanin, V., & Marinković, S. (2010). Recycled Concrete as Aggregate for Structural Concrete Production. *Sustainability, 2*(5), 1204-1225. https://www.mdpi.com/2071-1050/2/5/1204

[17] Manzi, S., Mazzotti, C., & Bignozzi, M. C. (2013). Short and long-term behavior of structural concrete with recycled concrete aggregate. *Cement and Concrete Composites, 37*, 312-318. doi:https://doi.org/10.1016/j.cemconcomp.2013.01.003.

[18] Limbachiya, M., Meddah, M. S., & Ouchagour, Y. (2012). Use of recycled concrete aggregate in fly-ash concrete. *Construction and Building Materials, 27*(1), 439-449. doi:https://doi.org/10.1016/j.conbuildmat.2011.07.023

[19] Marinković, S., Radonjanin, V., Malešev, M., & Ignjatović, I. (2010). Comparative environmental assessment of natural and recycled aggregate concrete. *Waste Management, 30*(11), 2255-2264. doi:https://doi.org/10.1016/j.wasman.2010.04.012

[20] Rao, A., Jha, K. N., & Misra, S. (2007). Use of aggregates from recycled construction and demolition waste in concrete. *Resources, Conservation and Recycling, 50*(1), 71-81. doi:https://doi.org/10.1016/j.resconrec.2006.05.010

[21] de Brito, J., Ferreira, J., Pacheco, J., Soares, D., & Guerreiro, M. (2016). Structural, material, mechanical and durability properties and behaviour of recycled aggregates concrete. *Journal of Building Engineering, 6*, 1-16. doi:https://doi.org/10.1016/j.jobe.2016.02.003

[22] Al Ajmani, H., Suleiman, F., Abuzayed, I., & Tamimi, A. (2019). Evaluation of Concrete Strength Made with Recycled Aggregate. *Buildings, 9*(3), 56. https://www.mdpi.com/2075-5309/9/3/56

[23] Xiao, J., Li, J., & Zhang, C. (2005). Mechanical properties of recycled aggregate concrete under uniaxial loading. *Cement and Concrete Research, 35*(6), 1187-1194. doi:https://doi.org/10.1016/j.cemconres.2004.09.020

[24] Butler, L., West, J. S., & Tighe, S. L. (2013). Effect of recycled concrete coarse aggregate from multiple sources on the hardened properties of concrete with equivalent compressive strength. *Construction and Building Materials, 47*, 1292-1301. doi:https://doi.org/10.1016/j.conbuildmat.2013.05.074

[25] *ACI Committee 318 (1995). Building code requirements for structural concrete and commentary,* American Concrete Institute, Farmington Hills, MI.

[26] CSA (2004). *Design of concrete structures*. *Standard CSA-A23.3– 04.* Canadian Standard Association, Mississauga, Ontario.

[27] British Standard Institution (2015). *BS 8500-2:2015*, in *Concrete–Complementary British Standard to BS EN 206–1–Part 2: Specification for Constituent Materials and Concrete.* British Standard Institution London, United Kingdom. p. 42.

[28] Junak, J., & Sicakova, A. (2017). Effect of Surface Modifications of Recycled Concrete Aggregate on Concrete Properties. *Buildings, 8*. doi:10.3390/buildings8010002

[29] Wang, R., Yu, N., & Li, Y. (2020). Methods for improving the microstructure of recycled concrete aggregate: A review. *Construction and Building Materials, 242*, 118164. doi:https://doi.org/10.1016/j.conbuildmat.2020.118164

[30] Dilbas, H., Simsek, M., & Çakır, Ö. (2014). An investigation on mechanical and physical properties of recycled aggregate concrete (RAC) with and without silica fume. *Construction and Building Materials, 61*, 50–59. doi:10.1016/j.conbuildmat.2014.02.057

[31] Song, X., Qiao, P., & Wen, H. (2015). Recycled aggregate concrete enhanced with polymer aluminium sulfate. *Magazine of Concrete Research, Paper 1400119*, 1-7. doi:10.1680/macr.14.00119

[32] Spaeth, V., & Djerbi Tegguer, A. (2013). Improvement of recycled concrete aggregate properties by polymer treatments. *International Journal of Sustainable Built Environment, 2*(2), 143-152. doi:https://doi.org/10.1016/j.ijsbe.2014.03.003

[33] Katkhuda, H., & Shatarat, N. (2017). Improving the mechanical properties of recycled concrete aggregate using chopped basalt fibers and acid treatment. *Construction and Building Materials, 140*, 328-335. doi:https://doi.org/10.1016/j.conbuildmat.2017.02.128

[34] Ali, B. (2019). Effect of aqueous sodium silicate on properties of recycled aggregate mortar. *SN Applied Sciences, 1*(10), 1296. doi:10.1007/s42452-019-1342-2

[35] Shi, C., Li, Y., Zhang, J., Li, W., Chong, L., & Xie, Z. (2016). Performance enhancement of recycled concrete aggregate – A review. *Journal of Cleaner Production, 112*, 466-472. doi:https://doi.org/10.1016/j.jclepro.2015.08.057

[36] Ignjatović, I. S., Marinković, S. B., Mišković, Z. M., & Savić, A. R. (2013). Flexural behavior of reinforced recycled aggregate concrete beams under short-term loading. *Materials and Structures, 46*(6), 1045-1059. doi:10.1617/s11527-012-9952-9

[37] Ignjatović, I. S., Marinković, S. B., & Tošić, N. (2017). Shear behaviour of recycled aggregate concrete beams with and without shear reinforcement. *Engineering Structures, 141*, 386-401.

[38] El Maaddawy, T., & Soudki, K. (2005). Carbon-Fiber-Reinforced Polymer Repair to Extend Service Life of Corroded Reinforced Concrete Beams. *Journal of Composites for Construction*, 9. doi:10.1061/(ASCE)1090-0268(2005)9:2(187)

[39] Tippakdee, S., Aosai, P., Chareanrit, P., Rammanee, N., Inmontien, N., & Imjai, T. (2022). Innovative precast concrete slabs made from recycled concrete reinforced with FRPs for stockyard constructions. *The Journal of King Mongkut's University of Technology North Bangkok, 35*.

[40] Shehata E, Morphy R, Rizkalla S. (2000). Fiber reinforced polymer shear reinforcement for concrete members: Behavior and design guidelines. *Canadian Journal of Civil Engineering* 27, 859–72.

[41] Hansapinyo C, Pimanmas A, Maekawa K, Chaisomphob T. (2003). Proposed Model of Shear Deformation of Reinforced Concrete Beam After Diagonal Cracking. *Journal of Materials, Concrete, Structures and Pavements*, JSCE, 58, 305-19.

[42] Ueda T, Sato Y, Ito T, Nishizono K. (2002). Shear Deformation of Reinforced Concrete Beam. *Journal of Materials, Concrete, Structures and Pavements*, JSCE, 56, 205-15.

[43] Al-Nini, A., Nikbakht, E., Syamsir, A., Shafiq, N., Mohammed, B.S., Al-Fakih, A., Al-Nini, W. and Amran, Y.M. (2020). Flexural behavior of double-skin steel tube beams filled with fiber-reinforced cementitious composite and strengthened with CFRP sheets. *Materials*, 13(14), 3064.

[44] Rahim, N.I., Mohammed, B.S., Al-Fakih, A., Wahab, M.M.A., Liew, M.S., Anwar, A. and Amran, Y.M. (2020). Strengthening the structural behavior of web openings in RC deep beam using CFRP. *Materials*, 13(12), 2804.

[45] Al-Fakih, A., Hashim, M. H. M., Alyousef, R., Mutafi, A., Sabah, S. H. A., & Tafsirojjaman, T. (2021, October). Cracking behavior of sea sand RC beam bonded externally with CFRP plate. *Structures* (Vol. 33, pp. 1578-1589). Elsevier.

[46] Imjai, T., Guadagnini, M., Garcia, R., & Pilakoutas, K. (2016). A practical method for determining shear crack induced deformation in FRP RC beams. *Engineering Structures, 126*, 353–364. doi:10.1016/j.engstruct.2016.08.007

[47] Younis, A., Ebead, U., Suraneni, P., & Nanni, A. (2020). Short-term flexural performance of seawater-mixed recycled-aggregate GFRP-reinforced concrete beams. *Composite Structures*, 236, 111860.

[48] ACI Committee 440 (2015). *Guide for the Design and Construction of Structural Concrete Reinforced with Firber-Reinforced Polymer (FRP) Bars (ACI 440.1R-15),* American Concrete Institute, Farmington Hills, MI.

[49] ACI Committee 211 (1991). *Standard practice for selecting proportions for normal, heavyweight, and mass concrete.* American Concrete Institute, Farmington Hills, MI.

[50] BS EN 12390-3 (2019). *Testing hardened concrete Part 3: Compressive strength of test specimens*, British Standards Institution, London UK.

[51] BS EN 12390–6 (2020). *Testing hardened concrete Part 6: Tensile splitting strength of test specimens*, British Standards Institution, London UK.

[52] BS EN 12390–5 (2019). *Testing hardened concrete Part 5: Flexural strength of test specimens*. British Standards Institution, London UK.

[53] BS EN 1992-1-1 (2004). *Eurocode 2: Design of concrete structures, Part 1-1: General rules and rules for buildings.* British Standards Institution, London UK.

[54] Kani, M. W., Huggins, M. W., Kani, G., & Wittkopp, R. R. (1979). *Kani on Shear in Reinforced Concrete*, Department of Civil Engineering, University of Toronto.

[55] Bischoff, P. (2007). Deflection Calculation of FRP Reinforced Concrete Beams Based on Modifications to the Existing Branson Equation. *Journal of Composites for Construction,* 11. doi:10.1061/(ASCE)1090-0268(2007)11:1(4)

[56] Bischoff, P., & Gross, S. (2010). Equivalent Moment of Inertia Based on Integration of Curvature. *Journal of Composites for Construction*, 15. doi:10.1061/(ASCE)CC.1943-5614.0000164

[57] Al-Sunna, R., Pilakoutas, K., Hajirasouliha, I., & Guadagnini, M. (2012). Deflection behaviour of FRP reinforced concrete beams and slabs: An experimental investigation. *Composites Part B: Engineering, 43*(5), 2125-2134. doi:https://doi.org/10.1016/j.compositesb.2012.03.007

[58] Abaqus/CAE: FEA software and user's manual version 6.14. 2014: Rhode Island, USA

[59] Alfarah, B., López-Almansa, F., & Oller, S. (2017). New methodology for calculating damage variables evolution in Plastic Damage Model for RC structures. *Engineering Structures, 132*, 70-86. doi:https://doi.org/10.1016/j.engstruct.2016.11.022

[60] Youssf, O., ElGawady, M. A., Mills, J. E., & Ma, X. (2014). Finite element modelling and dilation of FRP-confined concrete columns. *Engineering Structures, 79*, 70-85. doi:https://doi.org/10.1016/j.engstruct.2014.07.045

[61] Liu, W., Xu, M., & Chen, Z. (2014). Parameters calibration and verification of concrete damage plasticity model of Abaqus. *Industrial Construction, 44*(S1), 167-171.

[62] Taerwe, L., & Matthys, S. (2013). *fib* Model Code for concrete structures 2010. Berlin, Germany: Ernst & Sohn, Wiley. https://doi.org/10.1002/9783433604090 *2010*.

[63] Krätzig, W. B., & Pölling, R. (2004). An elasto-plastic damage model for reinforced concrete with minimum number of material parameters. *Computers and Structures, 82*(15), 1201-1215. doi:https://doi.org/10.1016/j.compstruc.2004.03.002

[64] Hordijk, D. A. (1992). Tensile And Tensile Fatigue Behaviour of Concrete; Experiments, Modelling And Analyses. *Heron Journal*, 37(1), 1-79.

[65] Xiao, J., & Falkner, H. (2007). Bond behaviour between recycled aggregate concrete and steel rebars. *Construction and Building Materials, 21*(2), 395-401.